β-Endorphin Expression in the Mouse Retina

Shannon K. Gallagher,[1] Paul Witkovsky,[2] Michel J. Roux,[3] Malcolm J. Low,[4] Veronica Otero-Corchon,[4] Shane T. Hentges,[1] and Jozsef Vigh[1]*

[1]Department of Biomedical Sciences, Colorado State University, Fort Collins, Colorado 80523, USA
[2]Department of Ophthalmology, New York University School of Medicine, New York, New York 10016, USA
[3]Department of Neurobiology and Genetics, IGBMC, CNRS UMR 7104, Inserm U 964, Université de Strasbourg, F-67404 Illkirch, France
[4]Department of Molecular and Integrative Physiology, University of Michigan, Ann Arbor, Michigan 48109, USA

ABSTRACT

Evidence showing expression of endogenous opioids in the mammalian retina is sparse. In the present study we examined a transgenic mouse line expressing an obligate dimerized form of Discosoma red fluorescent protein (DsRed) under the control of the pro-opiomelanocortin promoter and distal upstream regulatory elements to assess whether pro-opiomelanocortin peptide (POMC), and its opioid cleavage product, β-endorphin, are expressed in the mouse retina. Using double label immunohistochemistry we found that DsRed fluorescence was restricted to a subset of GAD-67-positive cholinergic amacrine cells of both orthotopic and displaced subtypes. About 50% of cholinergic amacrine cells colocalized DsRed and a large fraction of DsRed-expressing amacrine cells was positive for β-endorphin immunostaining, whereas β-endorphin-immunoreactive neurons were absent in retinas of POMC null mice. Our findings contribute to a growing body of evidence demonstrating that opioid peptides are an integral component of vertebrate retinas, including those of mammals. J. Comp. Neurol. 518:3130–3148, 2010.

INDEXING TERMS: retina; β-endorphin; starburst amacrine cell; POMC

In vertebrate retinas, neural processing of light signals is mediated primarily by the amino acid transmitters glutamate, gamma amino butyric acid (GABA), and glycine, with additional contributions from amines such as acetylcholine, dopamine and 5-hydroxytryptamine (reviewed in Ehinger, 1982). This short list, however, does not include a number of additional chemical messengers that influence retinal signal processing, for the retina also contains about 50 identified neuroactive peptides (reviewed in Brecha, 2003). In this study we focus on the retinal distribution of an opioid peptide, β-endorphin, and its precursor protein pro-opiomelanocortin (POMC).

The great diversity of the retinal peptide population has made it difficult to formulate a general framework for the roles peptides play in retinal operation, but some generalizations can be made about peptide organization and function. Many of the identified retinal peptides have been shown to coexist with an amino acid or amine cotransmitter (Vaney et al., 1989; Casini and Brecha, 1992; Cuenca and Kolb, 1998; Hannibal et al., 2000), consistent with observations in other parts of the central nervous system (CNS) reporting co-release of classical neurotransmitters and peptides from the same neuron (Hökfelt et al., 2000). Moreover, almost all the retinal peptides are found in inner retinal neurons, particularly in subtypes of amacrine cell (Brecha, 2003).

Endogenous opioid peptides possess a shared N-terminal tetrapeptide sequence Tyr-Gly-Gly-Phe and are divided into three families, originating from three large precursor proteins. Proenkephalin gives rise to two pentapeptide proteins, leu-enkephalin and met-enkephalin, the heptapeptide met-enkephalin-7, and the octapeptide met-enkephalin-8. Prodynorphin is cleaved to generate dynorphin A/B and α-neoendorphin (reviewed in Khalap et al., 2005). The alternative cleavage products of pro-opiomelanocortin include the opioid β-endorphin, the melanocortins adrenocorticotropic hormone (ACTH),

Grant sponsor: Richard H. Chartrand Foundation (to P.W.); Grant sponsor: HFSP; Grant number: RGY0004/2003 (to M.J.R.); Grant sponsor: National Institutes of Health (NIH); Grant number: NIH 2R01DK066604 (to M.J.L.); Grant number: NIH R01DK078749 (to S.T.H.); Grant number: R01 EY019051 (to J.V.).

*CORRESPONDENCE TO: Jozsef Vigh, Department of Biomedical Sciences, Colorado State University, Fort Collins, CO 80523.
E-mail: Jozsef.Vigh@Colostate.edu

Received October 14, 2009; Revised January 27, 2010; Accepted March 3, 2010
DOI 10.1002/cne.22387
Published online March 23, 2010 in Wiley InterScience (www.interscience.wiley.com)

α-, β-, and γ-melanocyte stimulating hormone (α-MSH, β-MSH, and γ-MSH, respectively) and the corticotropin-like intermediate lobe peptide (CLIP) (Millington, 2007). Each opioid peptide family preferentially binds to specific peptide receptors, known as mu-, delta-, and kappa-opioid receptors (μ-OR, δ-OR, and κ-OR, respectively). Although there is no absolute peptide/receptor pair specificity, β-endorphin binds preferentially to the μ-OR, the enkephalins show highest affinity for the δ-OR, and the dynorphin family for the κ-OR (Kieffer, 1995).

Most research on retinal opioid peptides has been done on fish and avian retinas (Djamgoz et al., 1981; Seltner et al., 1997; Fischer et al., 1998) and the majority of this work has focused on enkephalins, which are found in amacrine cells that colocalize GABA or glycine (Watt et al., 1988) and also the peptides somatostatin and neurotensin (Yang et al., 1997). With regard to mammalian retinas, Altschuler et al. (1982) provided immunocytochemical evidence for the presence of enkephalin in inner retinal neurons of the guinea pig retina, but functional studies of enkephalin actions in mammalian retinas are lacking.

Only sparse data exist for the presence or function of endorphin-like peptides and their receptors in mammalian retinas. Medzihradsky (1976) found that rat retinal homogenates showed stereospecific binding of etorphine, a synthetic, nonselective analog of morphine. Binding studies with the nonselective opioid receptor ligand [^{3}H]diprenorphine showed saturable specific binding in the rabbit retina (Slaughter et al., 1985). However, further analysis of binding site subtypes was precluded by the low density of binding sites. Wamsley et al. (1981), using [^{3}H]dihydromorphine, found autoradiographic labeling over the inner plexiform and ganglion cell layers (IPL and GCL, respectively) in rat and monkey retinas. Since dihydromorphine shows a 10 times higher affinity for μ-OR compared to δ-ORs, high affinity binding of dihydromorphine suggests the presence of μ-ORs in these retinas. Similarly, [^{3}H]naloxone binding indicated that μ-ORs are present in bovine retinal homogenates: specific [^{3}H]naloxone binding was most completely inhibited by the μ-OR specific compound, levorphanol ($IC_{50} = 1$ nM) (Borbe at al, 1982).

Given the weak database for opioid peptides and receptors in mammalian retinas, we decided to take advantage of a transgenic mouse model in which Discosoma red fluorescent protein (DsRed) is expressed under the transcriptional control of the mouse POMC gene promoter and neuronal regulatory elements (Hentges et al., 2009). In this transgenic mouse we found that POMC-DsRed expression was confined to cholinergic amacrine cells. Additionally, we demonstrated by immunocytochemistry that the opioid POMC cleavage product β-endorphin was located within cholinergic amacrine cells, whereas immunoreactivity for the alternative melanocortin cleavage products, ACTH and α-MSH, was not detected in inner retina. We provide quantitative data on the fractions of the cholinergic amacrine cell population which express β-endorphin. In a brief report, Brecha et al. (1995), utilizing an antibody against the μ-OR, found immunoreactivity in ganglion cell bodies and dendrites of the rat retina. Our data, in conjunction with the report of Brecha et al. (1995), suggest a close spatial apposition of β-endorphin release and binding sites in inner retina, thus providing an initial anatomical framework for further study of opioid peptide function in mammalian retinas.

MATERIALS AND METHODS

Animals

Wildtype C57BL/6J mice were obtained from Jackson Laboratories (Bar Harbor, ME). The POMC-DsRed transgenic mouse line (Hentges et al., 2009) was used to assess POMC promoter-driven expression of the red fluorescent protein DsRed. Tissue from POMC knockout mice (Smart et al., 2006) was used as a negative control for specificity of the β-endorphin antiserum. Mice were kept on a 12-hour light:dark cycle with lights on at 6:00 AM, fed standard chow and water ad libitum. Adult male and female mice were used for experimentation. Animals were handled in compliance with the Colorado State University Institutional Animal Care and Use Committee and all procedures met United States Public Health Service Guidelines.

Production of transgenic mice

Mice expressing the tdimer2(12) engineered form of DsRed (Campbell et al., 2002) under the control of pro-opiomelanocortin gene (*Pomc*) regulatory elements were produced by standard techniques and validated as described elsewhere (Hentges et al., 2009). In brief, the transgene contained 11.8 kb of mouse *Pomc* genomic sequences extending from nucleotide positions −13.3 kb to +3.2 kb, numbered relative to the transcriptional start site, that includes two distal neuronal regulatory enhancers (deSouza et al., 2005), the proximal promoter, exon 1, and intron 1. The 5′ flanking sequences were modified by an internal deletion of 4.7 kb ranging from positions −6.8 kb to −2.1 kb that were shown previously to be unnecessary for neuronal expression of transgenes (deSouza et al., 2005). Tdimer2(12) coding sequences followed by SV40T antigen transcriptional stop and polyadenylation signals were ligated to the *Pomc* sequences at a *Sma*I restriction site engineered into the 5′ UTR of exon 2 at nucleotide position +3.2 kb. The transgene DNA was purified from its pBlueScript (Stratagene, La

Jolla, CA) plasmid vector backbone after restriction endonuclease digestion at unique polylinker sites on both sides of the cloned insert and used for nuclear microinjection into fertilized one-cell mouse embryos. In some experiments, POMC-DsRed transgenic mice were further crossed with a glutamic acid decarboxylase (GAD)-67 enhanced green fluorescent protein (EGFP) transgenic mouse line (Tamamaki et al., 2003). The GAD67-EGFP transgene faithfully labels GABAergic neurons. In these mice, EGFP colocalizes with GAD67, GABA, and neuropeptides that are expressed in central nervous system (CNS) GABAergic neurons (neuron-nuclear specific protein, calretinin, parvalbumin, and somatostatin; Tamamaki et al., 2003). Furthermore, in the retinas of the GAD67-EGFP strain, most (99%) of the EGFP+ cells colocalize GABA (May et al., 2008). Genotyping of the compound transgenic mice with double-labeled POMC- and GAD67-expressing cells (Hentges et al., 2009) was performed using polymerase chain reaction (PCR) and primer sets specific for the EGFP and DsRed transgenes. Generation and breeding of neuronal-specific POMC-KO mice were described in detail elsewhere (Smart et al., 2006). In brief, transgenic mice were generated with a modified genomic construct predicted to express POMC in pituitary cells, but not in neurons. A 9.7-kb *Eco*RI-*Eco*RI mouse genomic DNA fragment containing the 3 *Pomc* exons and proximal promoter elements was subcloned into pBluescript SK (Stratagene) and used to construct the pituitary-specific POMC rescue transgene pHalEx2* (*Tg*), which contains a unique oligonucleotide sequence inserted into the 5′ UTR of exon 2 to provide a probe for specific detection of mRNA transcribed from the transgene, but not from endogenous *Pomc* alleles. The novel strain of transgenic mice was generated by nuclear microinjection of linearized pHalEx2* Tg DNA into B6D2 F2 hybrid 1-cell embryos. The pHalEx2* Tg allele was backcrossed from a single identified founder to inbred C57BL/6J mice (Jackson Laboratory) for two consecutive generations and subsequently crossed onto the $Pomc^{-/-}$ genetic background by an additional two generations of double-heterozygous matings. Genotyping was performed by PCR.

Immunohistochemistry

Mice were killed between 10:00 and 14:00 hours by exposure to CO_2 followed by cervical dislocation, or were deeply anesthetized with isoflurane and decapitated before both eyes were enucleated. A small incision was made at the ora serrata and the whole eye was fixed at room temperature in freshly prepared 4% paraformaldehyde in 0.1 M phosphate-buffered saline (PBS; pH 7.35) for 15 minutes. The cornea and lens were removed and the eyecups left in the same fixative solution for an additional 5 minutes.

Both whole-mounted retinas and cryostat-sectioned retinas were used for immunohistochemistry. For whole-mounts, isolated retinas were washed 3 × 15 min in 0.1 M PBS at room temperature, then incubated in blocking solution (0.3% Triton X-100 v/v, 0.1% sodium azide w/v, and 1% bovine serum albumin w/v in PBS) for 1–2 hours at room temperature or overnight at 4°C. Retinas were incubated overnight in primary antibodies diluted in blocking solution (Table 1) at room temperature on a shaker table. Retinas were then washed (3 × 15 min) in PBS and incubated, either at room temperature for 2 hours or overnight at 4°C, in the appropriate secondary antibodies (Table 1). After a final 3 × 15-minute wash in PBS, retinas were mounted on glass slides in Vectashield (Vector Laboratories, Burlingame, CA).

For cryostat sections, fixed eye cups were cryoprotected in 30% sucrose overnight, embedded in OCT (Ted Pella, Redding, CA) and cut into 20-μm-thick vertical sections. Sections were mounted on glass slides and stored frozen until immunostained using the above protocol. For immunostaining of peptides, either a fluorescent secondary or 3,3′-diaminobenzidine (DAB) amplification was employed. For DAB amplification, sections were washed in PBS, then incubated in 1% hydrogen peroxide in PBS for 30–60 minutes. Slides were then washed in PBS, incubated in ABC complex (Vectastain ABC kit, Vector Laboratories) for 2 hours at room temperature, and subsequently in DAB solution (Peroxidase substrate kit DAB, Vector Laboratories) until optimal staining was obtained (5–10 minutes). Slides were washed in Tris-buffered saline (TBS; pH 7.4) and mounted in TBS or Vectashield.

Antibody specificity

ACTH

Highly purified, iodination-grade ACTH from rat pituitary glands was used as the immunogen for the production of an anti-ACTH antiserum in rabbit. Rat ACTH has 93% sequence homology with mouse (NCBI Blast). The purified antibody was provided by Dr. A.F. Parlow (parlow@humc.edu) of the National Hormone & Peptide Program (NHPP), who found that it did not crossreact with any other pituitary hormones. In mouse CNS (Hentges et al., 2009) it was found that anti-ACTH immunoreactivity (ir) was abolished by preadsorption to ACTH 1-39 and was absent in POMC null mice.

α-MSH

The polyclonal α-MSH antiserum was raised in sheep against an immunogen consisting of α-MSH conjugated to bovine thyroglobulin. The specificity of the α-MSH antibody was demonstrated in rat hypothalamus by Elias

TABLE 1.
Primary Antibodies Applied in the Current Study

Antibody	Antiserum	Immunogen	Source	Catalog #/Lot #	Dilution
Adrenocorticotropic hormone (ACTH)	Rabbit Anti-ACTH	Purified rat ACTH from frozen pituitary glands	National Hormone & Peptide Program, Torrance, CA	AFP-156102789	1:10,000
Alpha-Melanocyte Stimulating Hormone (α-MSH)	Rabbit Anti- α-MSH	α-MSH conjugated with bovine thyrogloulin	Millipore, Billerica, MA	AB5087/LV1447004	1:10,000
Beta Endorphin	Rabbit Anti-β-Endorphin	Synthetic, complete human β-Endorphin	National Hormone & Peptide Program, Torrance, CA	AFP-791579Rb	1:5,000-1:20,000
Calbindin	Rabbit Anti-calbindin, Polyclonal	Recombinant mouse calbindin	Millipore, Billerica, MA	AB1778/LV1463639	1:2,500
Calretinin	Rabbit Anti-calretinin, Polyclonal	Recombinant rat calretinin	Millipore, Billerica, MA	AB5054/LV1532272	1:5,000
Choline Acetyltransferase (ChAT)	Goat Anti-ChAT, Polyclonal	Human placental ChAT enzyme	Millipore, Billerica, MA	AB144P/LV1541569	1:200
Glutamate Decarboxylase -65 (GAD65)	Mouse Anti-GAD65	Purified rat GAD enzyme, 64kDa subunit, from brain	Developmental Studies Hybridoma Bank, University of Iowa, Iowa City, IA	GAD-6	1:1,000
Glycine Transporter 1 (GLYT-1)	Goat Anti-GLYT-1, Polyclonal	Synthetic rat GLYT-1 peptide fragment, KAQIPIVGSNGSSRLQDSRI	Millipore, Billerica, MA	AB1770/LV1392052	1:5,000-1:10,000

et al. (1998), who showed that preadsorption of the antibody with its immunogen resulted in loss of specific staining.

β-*Endorphin*

The β-endorphin antiserum was produced in rabbit by Dr. A. F. Parlow using the synthetic peptide YGGFMT SEKSQTPLVTLFKNAIIKNAYKKGE, corresponding to complete human β-endorphin. Human β-endorphin has 94% sequence homology to mouse. The specificity of this antiserum was confirmed in the present study using POMC null mice, in which anti-β-endorphin immunoreactivity was absent in hypothalamus and retina, but present in those tissues of wildtype mice.

Calbindin

The polyclonal anti-calbindin antibody was raised in rabbit against recombinant mouse calbindin-28k. Western blot analysis of human cerebellar homogenate with this antibody showed a single band of ≈28 kDa in size (Matilla et al., 2001) similar to manufacturer's Western blot analysis of mouse brain lysate. In the developing mouse retina, de Melo et al. (2003) used this antibody to immunolabel specifically retinal horizontal cells, consistent with the observation that calbindin-28k is a horizontal cell-specific marker in rod-dominant retinas (Hamano et al., 1990). Haverkamp and Wässle (2000) used an antibody raised against recombinant rat calbindin-28k (Rabbit anti-calbindin, Swant, Bellinzona, Switzerland) to show that besides horizontal cells, some amacrine and ganglion cells, as well as three prominent layers in the IPL, showed calbindin immunoreactivity in the mouse retina. This immunohistochemical staining pattern has been observed in the inner retina in both mouse and rat studies using various other anti-calbindin antibodies (Moon et al., 2005; Kielczewski et al., 2005, respectively) and it is in perfect agreement with our results (Fig. 3).

Calretinin

Recombinant rat calretinin was used for the production of an anti-calretinin polyclonal antiserum in rabbit. The rat calretinin has 99% amino acid sequence homology to mouse calretinin (NCBI Blast). In immunoblots of rat tissues it recognizes both calcium-bound and calcium-unbound forms of calretinin (manufacturer's specifications). The molecular mass of calretinin is 29 kDa, and Choi et al. (2010) showed that, in Western blots of dog olfactory bulb tissue, this antibody recognized a corresponding single band. An immunohistochemical study by de Melo et al. (2005) used this antibody as a marker for amacrine cells in the developing mouse retina. Gábriel and Witkovsky (1998) showed a similar labeling pattern in the adult rat retina, with calretinin+ amacrine cells located in both the inner nuclear layer (INL) and ganglion cell layer (GCL), and three distinct bands in the IPL. This calretinin immunolabeling is in agreement with what

Haverkamp and Wässle (2000) reported in the adult mouse retina, and with our results (Fig. 3).

Choline acetyltransferase (ChAT)

The antigen-affinity purified polyclonal anti-ChAT antibody was generated in goat using human placental ChAT enzyme. Human ChAT has 86% sequence homology to mouse ChAT (NCBI Blast). Its specificity was established in Western blots of rat brain and skeletal muscle, in which the antibody recognized a single band of 68–72 kD (Brunelli et al., 2005). In retina this antibody selectively stains a subtype of amacrine cell that also internalizes radioactive acetylcholine (Masland and Mills, 1979; Voigt, 1986).

Glutamic acid decarboxylase (GAD)65

Affinity-purified GAD65 from adult rat brain was used to raise an anti-GAD6 monoclonal antibody in mouse. Rat GAD65 has 98% amino acid sequence homology to mouse GAD65 (NCBI Blast). In Western blot analysis of rat brain this antibody recognized a single band at 59 kD (Chang and Gottlieb, 1988). The corresponding band was absent in Western blots of mouse brain tissue taken from a GAD65 null mouse (Yamamoto et al., 2003).

Glycine transporter 1 (GLYT-1)

A polyclonal anti-GLYT-1 antiserum was raised in goat using a synthetic peptide (Table 1), corresponding to amino acids 614–633 at the carboxy-terminus of cloned rat GLYT-1. This peptide sequence is 95% homologous to that of mouse. In our hands, preadsorption of the antibody with its immunogenic peptide completely abolished immunolabeling in the mouse retina.

For double immunolabeling experiments, preparations were tested with both sequential and concurrent immunohistochemical protocols, with no differences in staining patterns noted. Omission of the primary antibody/antibodies resulted in no immunoreactivity.

To verify that the DsRed transgene product was expressed in authentic POMC neurons and as a control for labeling in the retina, immunolabeling studies were performed in brain slices. Mice were deeply anesthetized and perfused transcardially with 4% paraformaldehyde in PBS. After perfusion, brains were postfixed in 4% paraformaldehyde for 24 hours at 4°C before sectioning. Brain slices (50 μm thick) including the hypothalamic arcuate nucleus were prepared on a vibratome. Nonspecific binding was reduced by incubating the sections in PBS containing 0.3% Triton-x and 3% normal goat serum for 30 minutes at room temperature. Sections were incubated in primary antibody overnight at 4°C. Antibody sources and concentrations are listed in Table 1. Sections were rinsed 3 × 15 minutes in PBS then exposed to a fluorescent secondary antibody for 2 hours at room temperature. The tissue was then rinsed and mounted on glass slides for imaging.

In situ hybridization

Eyes were fixed by immersion in PBS containing 4% paraformaldehyde for 1 hour at room temperature, then embedded in Shandon Cryomatrix (Anatomical Pathology International, Runcorn, UK) and frozen on dry ice. Cryosections (12 μm) were collected on RNAse treated SuperFrost Plus Slides (Fisher Scientific, Illkirch, France). Slides were then washed for 5 minutes in PBS, acetylated, and dehydrated in graded ethanol solutions (70%, 90%, and 100%). The antisense and sense probes were synthesized and digoxigenin-labeled from the template T9962 obtained from Genepaint (http://www.genepaint.org), using SP6 and T7 polymerase, respectively (Promega, Madison, WI), and Dig-UTP (Roche Diagnostics, Basel, Switzerland). The antisense probe targets position 3–967 from the POMC sequence, with the addition of a 105-base long poly A.

After a first step of proteinase K digestion (0.01 μg/mL in 50 mM Tris, 5 mM EDTA, 0.05% Tween-20, pH 8.0) in PBS, sections were prehybridized for 30 minutes in Hyb-mix solution (Ambion, Austin, TX), hybridized for 5 hours, 30 minutes at 64°C in Hyb-mix containing 300 ng/mL riboprobes, and labeled with an anti-digoxigenin antibody coupled to peroxidase (Roche Diagnostics).

Confocal laser microscopy

Fluorescent images were taken with a Zeiss LSM 510 confocal microscope (Carl Zeiss, Oberkochen, Germany) or with a Nikon PM 800 confocal microscope equipped with a digital camera controlled by the Spot software program (Diagnostic Instruments, Sterling Heights, MI). On both microscopes, to avoid crosstalk between laser channels, digital images were acquired separately from each laser channel and then merged. Digital files were further processed with deconvolution software (AutoQuant Imaging, Watervliet, NY). For whole-mounted retinas, confocal Z-stack images (200 × 200 μm, in a 5 × 5 matrix) were taken at 40× from the vitreal surface to the OPL in 3–4-μm steps. For vertically cryosectioned retinas, single images or Z-stack images were taken at 40× or 63× in 2–3-μm increments. For all acquisitions, sequential scans at the different wavelengths were performed. Brightness and contrast of images were adjusted in Photoshop CS3 (Adobe 10.1, San Jose, CA). All such adjustments were made uniformly to the entire digital image.

Quantification and data analysis

Images were compiled and analyzed using Zeiss LSM Images Examiner software (Carl Zeiss). Cell counts for each whole-mounted retina were obtained through

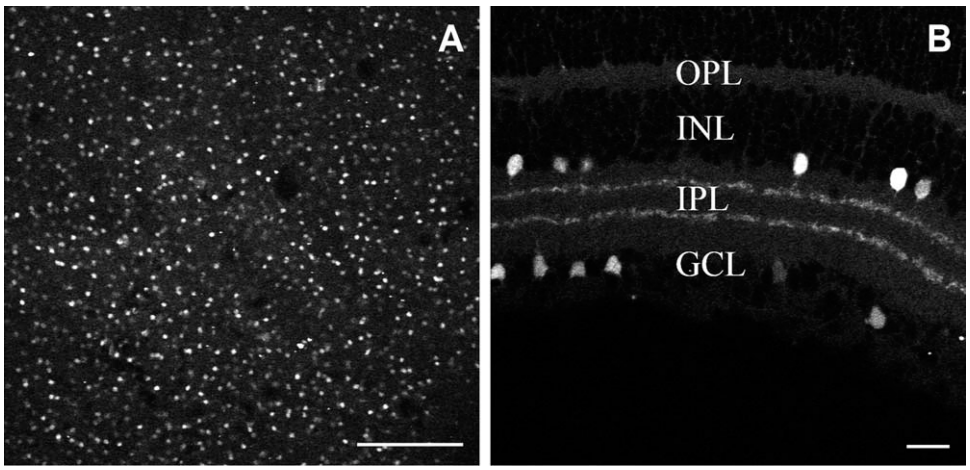

Figure 1. DsRed fluorophore expression in the retina of POMC transgenic mice in confocal images of whole-mounted (**A**) and vertically cryosectioned retinas (**B**). A: Low-power image of a POMC-DsRed retinal whole-mount focused on the INL, showing fluorescent cell bodies of similar shape, size, and distribution. B: Vertical cryostat section through the POMC-DsRed retina showing bright fluorescent cell bodies of similar shape and size distributed in both the INL and the GCL, with their processes forming two distinct bands within the IPL. Scale bars = 200 μm, in A; 20 μm in B.

compilation of Z-stack 40× images from both INL and GCL over 1 mm^2 areas in both central and peripheral retinal areas. Cell counts for cryostat sectioned retinas or whole-mounts were performed manually. Statistical analysis was done using a paired Student's *t*-test (Microsoft Excel, 2003); *P*-values ≤ 0.05 were considered significant. All graphs were generated with Sigma Plot (Sigma Plot 2001, Systat Software, Point Richmond, CA). Cumulative quantitative data are presented as averages ± SEM.

We performed a nearest-neighbor analysis (Wässle and Riemann, 1978) of DsRed+ cells on a representative retina obtained from a POMC-DsRed transgenic mouse as follows: Confocal images of five, 200 × 200 μm areas (quadrates) were randomly selected from both the peripheral and the central retina. Nearest-neighbor distances were measured with 0.1 μm resolution manually for all DsRed+ cells from center to center of the somas in these quadrates by using Zeiss LSM Images Examiner software (Carl Zeiss) in both the INL and GCL. The measurements in the five quadrates at similar eccentricity (i.e., central (C) or peripheral (P)) and within same cellular layers were plotted on histograms using 5 μm binning of the distances. Accordingly, four separate histograms (C-INL, C-GCL, P-INL, and P-GCL) were generated. Numbers of measurements/bin were normalized to the total number of measurements (*n*) within the area. The normalized histograms were fitted by a normal Gaussian function:

$$p(r) = k \exp[-1/2((r-\mu)/\sigma)^2]$$

where μ is the mean, σ is the standard deviation of the measurements, and k is a normalizing factor (Wässle and Riemann, 1978). The correlation between the histograms and the Gaussian fit (R^2: coefficient of determination) was calculated by Sigmaplot.

RESULTS

Distribution of POMC-DsRed+ cells in the retina

A transgenic mouse line was used to assess POMC promoter-driven red fluorophore (DsRed) expression in the retina (Hentges et al., 2009). In a low-magnification image of a whole-mounted POMC-DsRed mouse retina (Fig. 1A), numerous DsRed-expressing (DsRed+) somas were seen throughout the tissue. Vertical sections (Fig. 1B) revealed DsRed+ somas located either at the border of INL and IPL, or within the GCL. Two distinct DsRed+ bands were seen in the middle third portion of the IPL (Fig. 1B). No DsRed fluorescence was detected in the outer retina. All DsRed+ somas had a similar round shape and size (diameter 8.5 ± 1.0 μm; $n = 104$ taken from 12 retinas). At low magnification, DsRed fluorescence intensity in labeled somas appeared to be even across cells, indicating a similar expression level of the fluorophore, although no quantification was attempted on this point. The apparent differences in the brightness of DsRed fluorescence among immunostained somas (Fig. 1A) resulted from slight differences in the plane of optical sectioning through the imaged cells.

To obtain the retinal density of DsRed+ somas/mm^2, cell counts were carried out on whole-mounted retinas (n = 9 from different animals from four different litters), in 5 × 5 adjacent quadrates, 200 × 200 μm each, at both the center (near the optic nerve) and at the retinal periphery, focusing at both the INL/IPL border and the GCL. Data

obtained from a single representative retina are illustrated in Figure 2A. Note the variability in the number of DsRed+ cells across quadrates: in the plotted example, cell counts in the INL varied between 29 and 66 in central retina, and between 28 and 63 in peripheral retina (averaging 47 ± 1.9 and 42 ± 1.7, respectively). Similarly, in the GCL, cell counts ranged from 17–37/quadrate in central retina and 21–39 in peripheral retina (averaging 27 ± 1.0 and 28 ± 1.6, respectively). In addition, we found variation in the average DsRed+ cell numbers/quadrate across animals: in the INL, ranging from 28–56 in central INL and 30–59 in peripheral INL (giving an overall average of 46 ± 0.8 and 42 ± 0.9, respectively). In the GCL the comparable variation across animals ranged from 23–48 in central retina and 17–43 in peripheral retina (averaging 32 ± 0.7 and 30 ± 0.7, respectively). Mean cell density/mm^2 values were obtained by summing cell numbers in 25 quadrates, for both the INL and the GCL in their respective locations and averaging those values across animals (n = 9). The analysis of cell density data is summarized in Figure 2B. We found that the density of DsRed+ somas in the INL was significantly higher than in the GCL in both the retinal center (1,182 ± 64/mm^2 vs. 803 ± 86/mm^2, $P < 0.00001$) and periphery (1,039 ± 87/mm^2 vs. 756 ± 77/mm^2, $P < 0.000009$, paired Student's *t*-test). Within their respective cellular layers, a slightly higher density of DsRed+ somas was found at the central INL and GCL than in the periphery, but the differences were statistically significant only in the INL (INL, $P < 0.02$; GCL: $P < 0.09$, paired Student's *t*-test).

Nearest-neighbor analysis (Wässle and Riemann, 1978) was performed to quantify the tiling regularity of the DsRed+ somas in the retina (for details, see Materials and Methods). Histograms generated from the nearest-neighbor distance data at each area (INL and GCL at both the center and periphery) were fit well by Gaussian functions (R^2 ranged from 0.89–0.98; Fig. 2), indicating that distances followed a normal distribution. The average distance between the nearest DsRed+ cells in the INL was 21.0 ± 7.0 μm (n = 290) at the center and 24.2 ± 7.5 μm (n = 207) at the periphery. The comparable average distances in the GCL were 21.6 ± 11.0 μm at the center and 24.9 ± 7.5 μm at the periphery (n = 195 and n = 182, respectively). The regularity of DsRed+ soma distribution given by the mean distance (μ) divided by the standard deviation (σ) (Wässle and Riemann, 1978) revealed higher regularity in the INL (R = 3.0 at the center and R = 3.2 at the periphery) than in the GCL (R = 1.9 at the center and R = 2.6 at the periphery).

To assess the position of the DsRed+ bands in the IPL, vertical sections of DsRed+ mouse retinas were immunostained for two calcium-binding proteins, calretinin and calbindin. Calretinin and calbindin are expressed in a congruent trilaminar pattern in the IPL of the mouse retina (Haverkamp and Wässle, 2000). We found that the inner DsRed+ band overlapped with the inner calretinin (Fig. 3A–C) and calbindin (Fig. 3D–F) strata between sublaminae 3 and 4, whereas the outer DsRed+ band in the IPL colocalized with the outermost strata of both calretinin and calbindin. Accordingly, the outer DsRed+ band is situated between sublaminae 1 and 2 (Ghosh et al., 2004).

The morphology of POMC-DsRed+ cells with somas in the INL suggested DsRed was expressed by amacrine cells. However, in the mouse retina about half of the cells in the GCL are ganglion cells and the other half are displaced amacrine cells (Jeon et al., 1998; Kong et al., 2005); therefore, the DsRed+ somas located in the GCL could be either amacrine or ganglion cells, or both. To examine further the identity of DsRed+ retinal neurons in both INL and GCL, we looked for colocalization of the DsRed signal with well-characterized neurochemical markers for amacrine cells.

POMC-DsRed+ cells in the retina are a subset of GABAergic amacrine cells

The mammalian retina has about 30 morphological subtypes of amacrine cell (MacNeil and Masland, 1998); half of them are glycinergic, the other half are GABAergic (Vaney, 1990). GABA and glycine have not been detected in the same amacrine cells in mammals (Marc et al., 1998; Haverkamp and Wässle, 2000).

In immunohistochemical studies the glycine transporter 1 (GLYT-1) is preferred to glycine as a marker for glycinergic amacrine cells over glycine, since some cone bipolar cells also contain glycine, whereas only glycinergic amacrine cells express GLYT-1 (Zafra et al., 1995; Vaney et al., 1998; Pow, 1998; Haverkamp and Wässle, 2000).

GLYT-1 immunolabeling was performed on vertical cryostat sections of POMC-DsRed mouse retinas. As shown in Figure 4A–C, DsRed+ cells did not colocalize with GLYT-1, indicating that DsRed+ cells in the mouse retina were not glycinergic amacrine cells.

In GABAergic neurons, including GABAergic amacrine cells, GABA is synthesized mainly via decarboxylation of glutamic acid by two isoforms of glutamic acid decarboxylases (GADs), distinguished according to their molecular masses, 65 and 67 kDa (GAD65 and GAD67, respectively). GABAergic amacrine cells in the mammalian retina can express either or both GAD isoforms (Vardi and Auerbach, 1995; Dkhissi et al., 2001; Andrade da Costa and Hokoc, 2003). We found that GAD65 immunostaining was confined to neuronal somas that lacked DsRed fluorescence (Fig. 4D–F). Furthermore, GAD65 immunolabeling was clearly absent from the DsRed+ IPL strata,

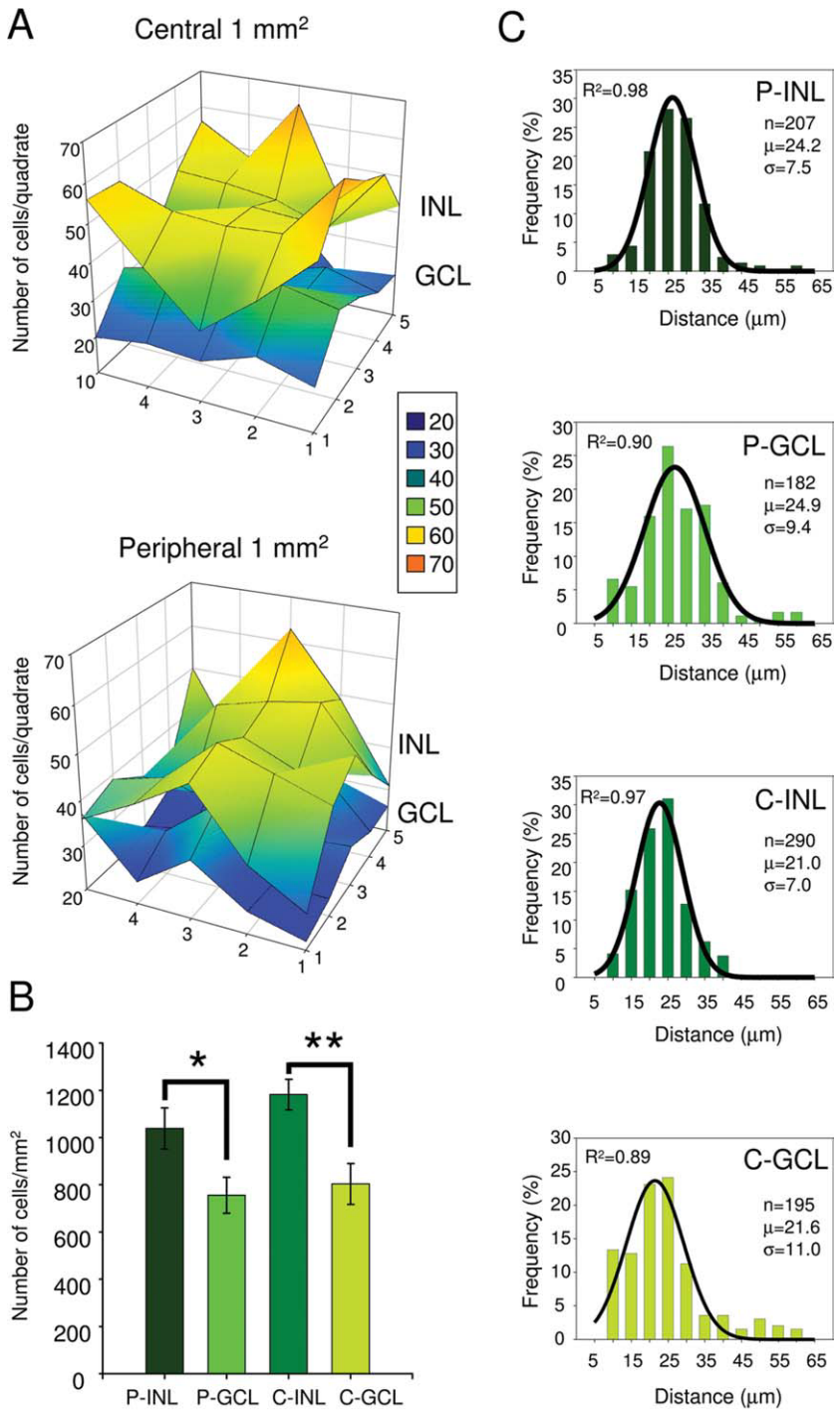

Figure 2. **A**: POMC-DsRed+ soma distribution in a single representative retina. Cell body counts were performed in the INL and GCL over a 1-mm^2 area compiled from 5 × 5, adjacent, 200 × 200 μm confocal Z-stack images at both the center (C) and at the periphery (P) of the retina. The 3D surface plot shows that despite small differences in the soma counts/quadrate, POMC-DsRed somas were rather evenly distributed in each nuclear layer. However, there are more DsRed+ somas in every INL quadrate than in the corresponding GCL area. The number of total DsRed+ cells/mm^2 plotted in this example: C-INL:1198; C-GCL:677; P-INL:1068; P-GCL:715. Inset shows how the number of cells counted in the 200 × 200 μm quadrates corresponds to colors used for the surface plot. **B**: Cumulative data (n = 9) showing POMC-DsRed soma distribution, comparing cell counts within nuclear layers in the periphery (P) and center (C) and between inner nuclear and ganglion cell layers of the mouse retina (i.e., P-INL, P-GCL, C-INL, and C-GCL, respectively); error bars represent SEM; $*P < 0.00001$; $**P < 0.000009$, paired Student's *t*-test. **C**: Histograms of the nearest-neighbor distances at (P) and (C) in both inner nuclear and ganglion cell layers of the mouse retina (i.e., P-INL, P-GCL, C-INL, and C-GCL, respectively). Bin size: 5 μm. Absolute numbers of observations/bin were normalized to the total number of measurements (n). Normalized histograms were fitted with Gaussian distribution functions (solid lines). R^2: coefficient of determination; μ: average of nearest-neighbor distances; σ: standard deviation.

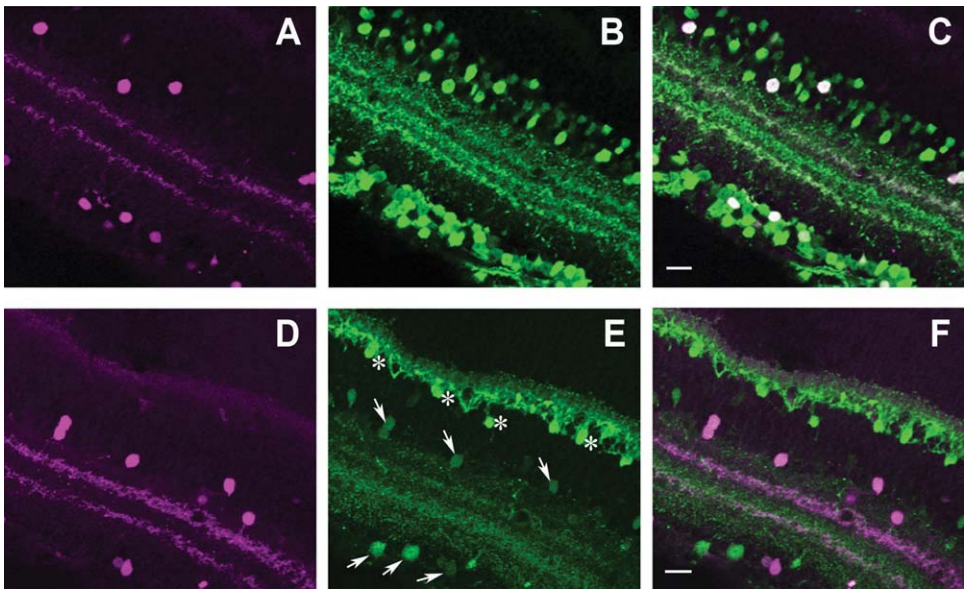

Figure 3. Calcium-binding proteins in POMC-DsRed+ cells in confocal images of vertical cryostat sections. **A,D**: POMC-DsRed (magenta) retina showing soma distribution in both the INL and GCL with two bands in the IPL. **B**: Confocal image illustrating the same region as in A, showing numerous calretinin+ (green) somas in the INL and GCL and three distinct bands within the IPL. **C**: A merged image of A and B showing colocalization of POMC-DsRed+ and calretinin+ somas, as well as colocalization of POMC-DsRed+ bands with the inner and outer calretinin+ IPL bands. **E**: Confocal image of the same region as in D, showing calbindin+ (green) somas in two distinct regions of the INL with somas also in the GCL and in three distinct bands in the IPL. The calbindin+ (putative horizontal cell) somas (asterisks) at the outer border of the INL and their projections seen in the OPL were more brightly stained than were somas and processes located in the inner retina (arrows). **F**: A merged image of D and E showing colocalization of POMC-DsRed+ somas and bands with calbindin+ somas and inner and outer IPL bands. Note, all POMC-DsRed+ somas and bands colocalize with calretinin and calbindin. Scale bars = 20 μm.

whereas other layers of the IPL were strongly labeled, indicating that GAD65 is transported to amacrine cell processes.

To assess the expression of GAD67 in POMC-DsRed+ amacrine cells, we crossed the POMC-DsRed line with a GAD67-EGFP knockin mouse line that marks GAD67-positive GABAergic neurons in the nervous system (Tamamaki et al., 2003) including the retina (May et al., 2008). In retinas of progeny carrying both GAD67-EGFP and POMC-DsRed constructs, cell counts were performed in whole-mounted retinas (n = 2) in 1 mm^2 areas divided into 200 × 200 μm quadrates, at the center and periphery in both INL and GCL. A total of 10,029 DsRed+ cells was counted (Table 2), of which 9,982 (99.5%) colocalized EGFP, i.e., virtually every POMC-DsRed+ cell was EGFP+. Examination of retinal cross-sections, moreover, revealed that the two DsRed+ bands in the IPL colocalized EGFP+ in GAD67-EGFP mice (Fig. 4G,H).

Retinal POMC-DsRed+ neurons are a subset of cholinergic amacrine cells

Cholinergic amacrine cells form two functional subpopulations in the mammalian retina: OFF types with somas located at the INL/IPL border whose processes arborize in a thin layer between sublaminae 1 and 2 of the IPL, and ON types with somas displaced to the GCL and whose processes arborize between IPL sublaminae 3 and 4 (Haverkamp and Wässle, 2000). The overall distribution of cholinergic amacrine cell somas and their processes was therefore very similar to that of POMC-DsRed+ amacrine cells. Furthermore, cholinergic amacrines colocalize calbindin and calretinin (Ghosh et al., 2004) as we found for POMC-DsRed+ retinal neurons. Therefore, we tested directly whether POMC-DsRed, and the cholinergic amacrine cell marker, ChAT-ir, colocalized. We observed that POMC DsRed+ somas colocalized ChAT in both GCL and INL (Fig. 5A–C). Consistent with the somatic colocalization, we found strong colabeling of both POMC-DsRed+ strata with ChAT in the IPL (Fig. 5D–F). Counts were performed on five whole-mounted retinas from five different POMC DsRed+ mice (see Materials and Methods). The data summarized in Table 3 revealed that essentially all POMC-DsRed+ cells were cholinergic in the POMC-DsRed retinas (16,439 out of 16,457 counted in total), but only ≈50% of all ChAT+ cells expressed DsRed signal.

POMC gene products expressed in DsRed+ hypothalamic neurons and in the pituitary

Although transgenic mice may reliably express a detectable level of fluorophore under neuronal promoter

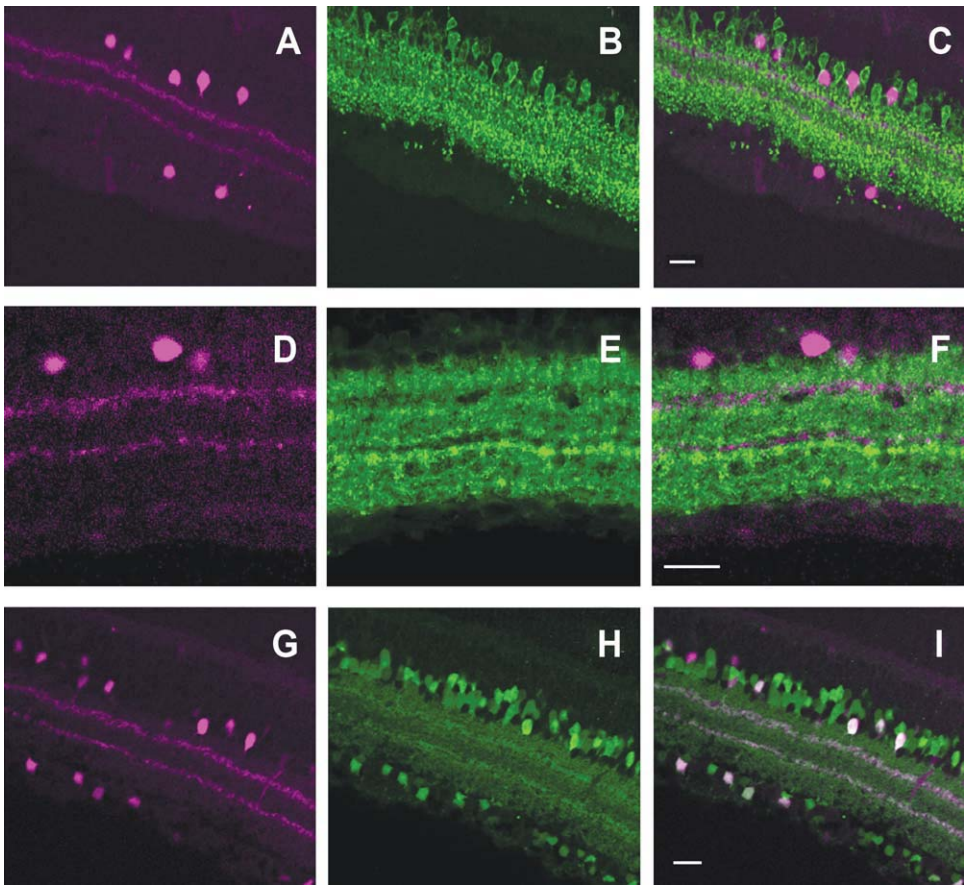

Figure 4. Inhibitory amacrine cell marker detection in POMC-DsRed cells in confocal images of vertical cryostat sections. **A,D**: POMC-DsRed (magenta) retina showing soma distribution in both the INL and GCL with two bands in the IPL. **B**: Image representative of the same region as A, showing GLYT-1 immunolabeling (green) for numerous cell bodies in the INL with projections throughout the IPL. Note the absence of GLYT-1-ir somas in the GCL. **C**: A merged image of A and B, showing no colocalization of POMC-DsRed+ cell bodies with GLYT-1 immunolabeling. Additionally, although GLYT-1+ projections are broadly distributed within the IPL, they do not colocalize with the two DsRed+ bands. **E**: Image displaying the same region as in D, showing faint GAD65+ somas (green) in the INL and GCL with widespread projections throughout most of the IPL. Note the two distinct bands characterized by an absence of GAD65+ projections in the IPL. **F**: A merged image of D and E showing no colocalization of GAD65-ir cell bodies or their projections with the two POMC-DsRed+ bands, which distribute within horizontal spaces in the IPL devoid of GAD65-ir. **G**: DsRed+ somas (magenta) and projections of a POMC-DsRed/GAD67-EGFP double transgenic mouse. **H**: Image illustrating the same region as in G, showing GAD67-EGFP+ somas in both the INL and the GCL and two bands within the IPL from their projections. **I**: A merged image of G and H showing strong colocalization of POMC-DsRed+ cell bodies in both the INL and GCL with GAD67-EGFP+ somas. Furthermore, colocalization of these markers in two IPL bands is also seen. Scale bars = 20 μm.

control, this result has to be further evaluated because of the complex regulation of such transgene expression. Multiple reports show great variation in promoter-driven fluorescent marker expression across brain areas (von Engelhardt et al., 2007; Caputi et al., 2009). In extreme cases, not only are the expression levels different, but the fluorophore can be expressed in cell populations in which the promoter does not normally drive expression in wildtype mice (ectopic expression). As a case in point, a ChAT-EGFP transgenic mouse line expresses EGFP in retinal amacrine cells having a different morphology than the cholinergic cells that would be expected to be labeled by the transgene (Haverkamp et al., 2009), although a good correspondence between EGFP and ChAT expression was found elsewhere in the brain of the same transgenic animals (von Engelhardt et al., 2007). Furthermore, the transgene containing the same *Pomc* regulatory elements as those used in the present report and an EGFP fluorophore reporter resulted in nearly perfect eutopic expression of EGFP in POMC neurons of the hypothalamus, but also ectopic expression in immature granule cell neurons of the dentate gyrus in the hippocampus (Overstreet et al., 2004).

Thus, neuronal expression of the DsRed fluorophore, although under the control of the POMC promoter, does not automatically indicate the expression of the large

precursor polyprotein POMC or any of its specific cleavage products (ACTH, β-endorphin, or α-MSH). To determine whether POMC gene products were expressed in the mouse retina, we performed immunohistochemical studies to examine possible colabeling of POMC-DsRed+ amacrine cells with antibodies directed against ACTH, β-endorphin, or α-MSH. As a positive control, identical immunostaining was carried out first on pituitaries and brain sections containing the arcuate nucleus of the hypothalamus from POMC-DsRed mice, since the expression of POMC products has been well documented in these regions (Bicknell, 2008).

TABLE 2.
DsRed+ Soma Counts in 2 Retinas of Progeny Carrying Both GAD67-EGFP and POMC-DsRed Constructs

	DsRed only (/mm^2)	DsRed+/ GAD67+ (/mm^2)	DsRed+/ GAD67+(%)
Retina1_Periphery_INL	2	1253	99.8
Retina2_Periphery_INL	15	1455	98.9
Retina1_Periphery_GCL	0	1091	100
Retina2_Periphery_GCL	15	1041	98.5
Retina1_Center_INL	4	1392	99.7
Retina2_Center_INL	1	1406	99.9
Retina1_Center_GCL	7	1214	99.4
Retina2_Center_GCL	3	1130	99.7

POMC-DsRed neurons showed specific immunoreactivity for ACTH, with nearly 100% overlap between DsRed and ACTH-ir in the hypothalamus, independent of the sex of mice used for the studies (Hentges et al., 2009). β-Endorphin and α-MSH antibodies also revealed immunoreactive products in DsRed+ hypothalamic neurons, but, for both antibodies, immunostaining was more prominent in fibers than in cell bodies (Fig. 6A). Inhibiting axonal transport by intraventricular (i.c.v.) injection of colchicine (Sigma, St. Louis, MO; 10 μg in 1 μL) 18 hours before tissue collection, greatly increased β-endorphin staining intensity in the somas of DsRed+ POMC neurons, confirming that the POMC-DsRed transgene labeled authentic POMC neurons (Fig. 6B). In the pituitary, both the β-endorphin and the ACTH antibodies labeled somas, some of which were DsRed+ (Fig. 6C,D, respectively). Importantly, all of the DsRed+ anterior lobe cells were corticotrophs because they were colabeled with one or the other POMC peptide antiserum.

DsRed+ retinal amacrine cells express β-endorphin

Whole-mounted DsRed-expressing retinas were treated with antibodies against ACTH, β-endorphin, or α-MSH as described above for the hypothalamic studies. Unlike the hypothalamus and pituitary, in retinal whole-mounts only

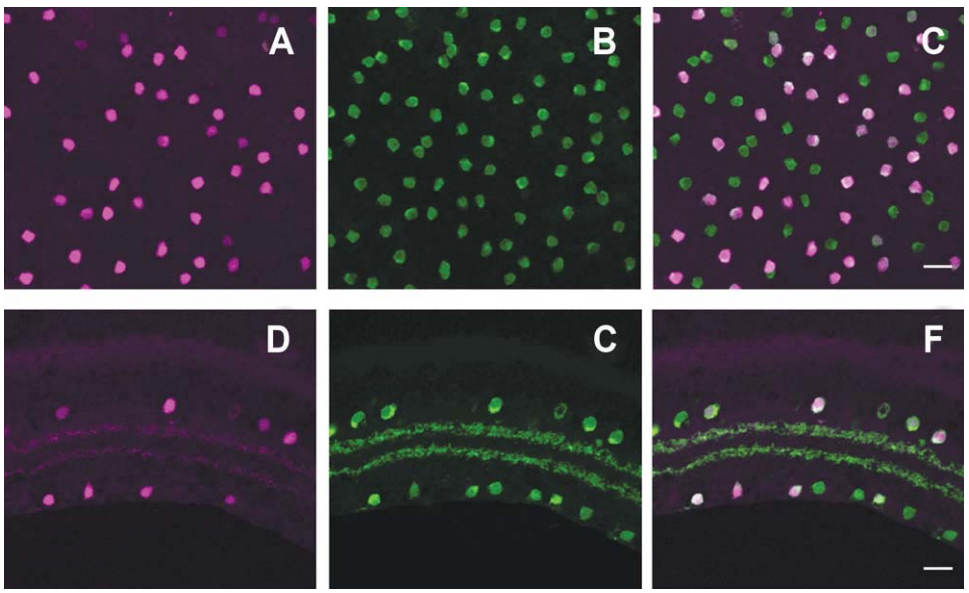

Figure 5. POMC-DsRed transgene colocalizes with the cholinergic amacrine cell marker ChAT in confocal images of retinal whole-mounts (**A–C**) and vertical cryostat section (**D–E**). A: High-power image of a whole-mounted POMC-DsRed (magenta) retina focused on the INL. B: Image illustrating the same region as A, showing numerous ChAT+ soma. C: A merged image of A and B, showing strong colocalization of POMC-DsRed+ cell bodies with ChAT (green). Note that not all ChAT+ somas are POMC-DsRed+. D: Vertical cryostat section through POMC DsRed (magenta) retina showing the distribution of labeled somas in both the INL and GCL and two bands of labeled processes in the IPL. E: Image of the same region as D, showing ChAT-ir cell bodies (green) evenly distributed within the INL and GCL and two distinct ChAT-ir bands in the IPL. **F**: A merged image of D and E demonstrating strong colocalization of POMC-DsRed+ somas and ChAT+ somas within the INL and GCL with further colocalization within two distinct bands of labeled processes in the IPL. Scale bars = 20 μm.

TABLE 3.
Summary of DsRed+ Soma Counts in 5 Retinas From 5 Animals Carrying POMC-DsRed Construct, Immunolabeled for ChAT

	DsRed+ total (/mm^2)	DsRed+/Chat+ (/mm^2)	Chat+ only (/mm^2)	Chat+ total (/mm^2)	DsRed+/ Chat+ (%)	Chat+/ DsRed+ (%)
Periphery_INL	918 ± 73	917 ± 73	887 ± 97	1,804 ± 89	51 ± 4	100 ± 0.04
Periphery_GCL	640 ± 68	640 ± 68	835 ± 106	1,475 ± 85	46 ± 5	100
Center_INL	1097 ± 77	1077 ± 77	977 ± 21	2,050 ± 72	53 ± 2	100 ± 0.1
Center_GCL	655 ± 53	654 ± 53	931 ± 45	1,586 ± 49	44 ± 3	100 ± 0.04

the β-endorphin antibody labeled POMC-DsRed+ amacrine cells. Cell counts were performed in two retinas over 1 mm^2, at the center in one of them and at the periphery in the other. The data are presented in Table 4. Most, but not all β-endorphin+ somas colocalized DsRed, whereas the percentage of POMC-DsRed expressing cells that colocalized β-endorphin varied between 0.1% and 6.1%, depending on retinal area: the highest degree of colocalization was observed in the INL at the periphery and the least was in the GCL at the center (Fig. 7A–C). Colchicine treatment either i.c.v. or directly into the posterior chamber of the eye (10 μg in 1 μL) 18 hours before tissue collection did not increase the number of β-endorphin+ somas in whole-mounted POMC-DsRed retinas ($n = 4$, not illustrated).

Immunostaining for β-endorphin also was performed on vertical cryostat sections of POMC-DsRed retinas using DAB amplification. As can be seen in Figure 7D–F, β-endorphin+ somas were located within the INL and GCL. Furthermore, most β-endorphin+ cells colocalized with POMC-DsRed+ cells within these cellular layers. Importantly, β-endorphin staining with DAB intensification in vertical retinal sections revealed more β-endorphin+ cells, and a higher colocalization percentage between POMC-DsRed and β-endorphin: ≈44% of DsRed+ somas were labeled for β-endorphin compared to the whole-mount data obtained with β-endorphin immunolabeling (6% at most). It is noteworthy that even with the DAB we did not detect β-endorphin-ir in all DsRed+ cells. DAB amplification did not reveal ACTH or α-MSH-immunopositive retinal cells under similar conditions (not illustrated).

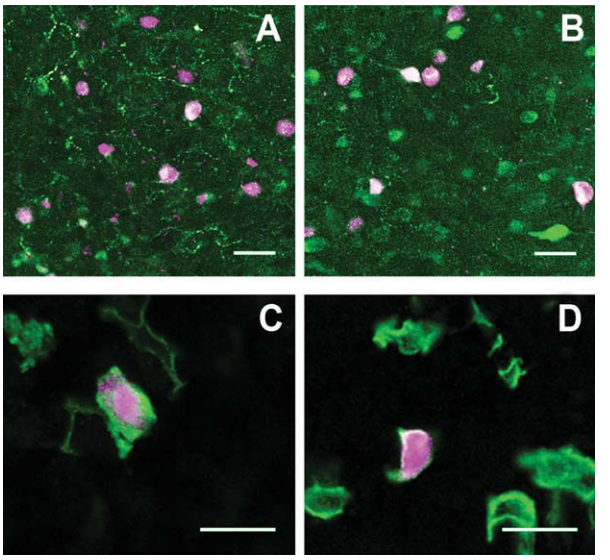

Figure 6. POMC-DsRed+ neurons in the arcuate nucleus and the pituitary show β-endorphin immunoreactivity. **A**: β-endorphin immunoreactivity (green) was limited to neuronal fibers and showed only weak immunoreactivity in cell bodies of DsRed+ hypothalamic neurons (magenta). **B**: Inhibiting axonal transport by colchicine increased β-endorphin immunoreactivity in the soma of DsRed+ POMC neurons. In the pituitary, DsRed+ cell (magenta) are immunolabeled for β-endorphin (**C**) and ACTH (**D**) (both green) without colchicine treatment. Scale bars = 20 μm.

POMC mRNA expression in wildtype mouse retina

To investigate whether *Pomc* promoter-driven DsRed expression in cholinergic amacrine cells was a byproduct of transgenic manipulation, we investigated POMC mRNA expression in wildtype mouse retina with in situ hybridization. POMC mRNA was reliably detectable in somas located at the inner border of the INL as well as in somas located in the GCL. A faint signal was occasionally visible in the outer part of INL, toward the OPL (Fig. 8A). We did not find POMC mRNA signal in the IPL. The control sense probe did not give any signal (Fig. 8B).

These results demonstrate that *Pomc* is expressed in the mouse retina. Moreover, the POMC mRNA signal location strongly supports the supposition that a fraction of cholinergic amacrine cell somas express POMC mRNA in the wildtype mouse, indicating that the red signal in the cholinergic amacrine cell of the POMC-DsRed mice was not ectopic. However, further studies are needed to completely rule out the possibility that some level of expression is ectopic.

Cholinergic amacrine cells express β-endorphin in wildtype, but not in the POMC knockout mouse retina

To assess whether cholinergic amacrine cells indeed express β-endorphin we performed double immunostaining

TABLE 4.

Summary of DsRed+ Soma Counts in 2 Retinas From 2 Animals Carrying POMC-DsRed Construct, Immonolabeled for β-endorphin

	DsRed+ total (/mm^2)	DsRed+/ βend+ (/mm^2)	βend+ only (/mm^2)	βend+ total (/mm^2)	βend+/ DsRed + (%)	DsRed+/ βend+ (%)
Retina1_Periphery_INL	1,279	79	14	93	6.1	84.9
Retina1_Periphery_GCL	937	35	16	51	3.7	68.6
Retina2_Center_INL	1,221	33	12	55	2.9	73.3
Retina2_Center_GCL	596	1	1	2	0.1	50

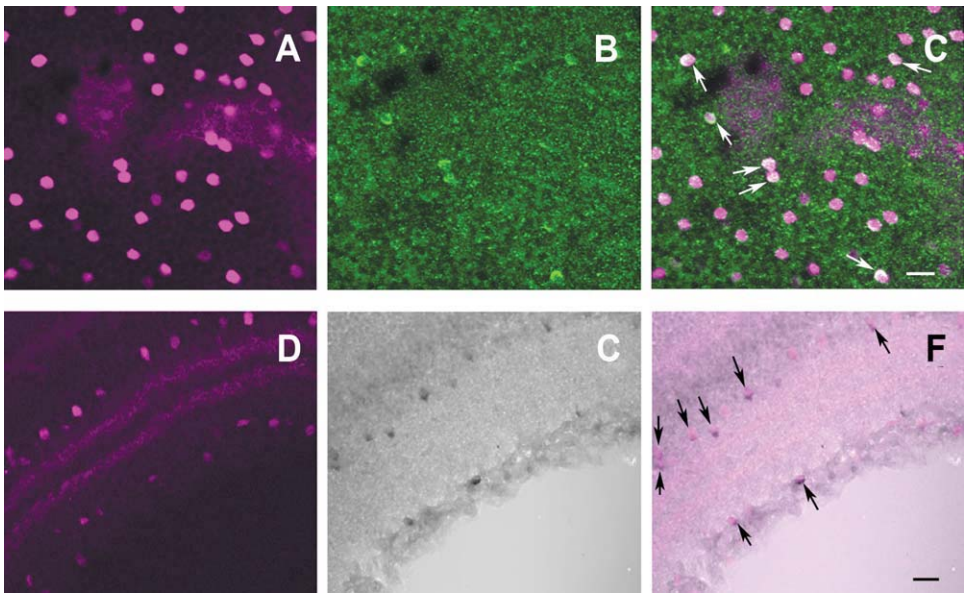

Figure 7. In the retina of POMC-DsRed transgenic mice a subset of DsRed+ amacrine cells colocalizes β-endorphin. **A**: High-power image of a whole-mounted POMC-DsRed (magenta) retina focused on the INL. **B**: Image displaying the same region as A, showing distinct β-endorphin+ cell bodies (green) of similar size and shape. **C**: A merged image of A and B, showing colocalization of β-endorphin and DsRed expression in somas (white arrows). **D**: Vertical cryostat section through POMC-DsRed (magenta) retina showing the distribution of labeled somas in both the INL and GCL with two bands in the IPL. **E**: DAB amplification of cryostat sectioned retinas for visualization of β-endorphin, illustrating the same region as D. Note β-endorphin-ir within somas in both the INL and GCL. **F**: A merged image of D and E, showing perfect colocalization of β-endorphin+ cell bodies with POMC-DsRed signal (black arrows). Note that not all DsRed+ cells show β-endorphin-ir. Scale bars = 20 μm.

for β-endorphin and ChAT on vertical cryostat sections of wildtype mouse retinas. As can be seen in Figure 9A–C, DAB-intensified β-endorphin staining occurs in wildtype retinas. Out of 132 β-endorphin cells 108 (82%) were also ChAT+. On the other hand, in the same retinal sections a total of 1,274 ChAT+ amacrine cells was counted; therefore, ≈9% of ChAT+ cells coexpressed β-endorphin in the wildtype mouse retina.

In contrast, in the retinas of POMC-KO mice no β-endorphin colabeling of ChAT+ retinal neurons in vertical cryostat sections was observed (compare Fig. 10A–C, to D–F; wildtype vs. POMC-KO, respectively). The number of β-endorphin+ fibers and somas is relatively high in the hypothalamus of both POMC-DsRed transgenic (Fig. 6B,C) and wildtype mice (Fig. 10G). No neuronal staining was observed for β-endorphin in the arcuate nucleus of POMC-KO mice (Fig. 10H), consistent with a lack of β-endorphin labeling in the retina of POMC-KO mice (Fig. 10E,F). These findings confirm the specificity of the β-endorphin antibody used in the present studies.

DISCUSSION

The present data demonstrate that expression of the POMC-DsRed transgene is almost exclusively confined to a well-defined class of retinal cells, the GAD67-positive, cholinergic amacrine cells. Furthermore, a sizeable fraction of the POMC-DsRed amacrine cells is immunoreactive for the opioid product, β-endorphin, but not for ACTH or α-MSH. Wildtype mouse retina also expresses POMC

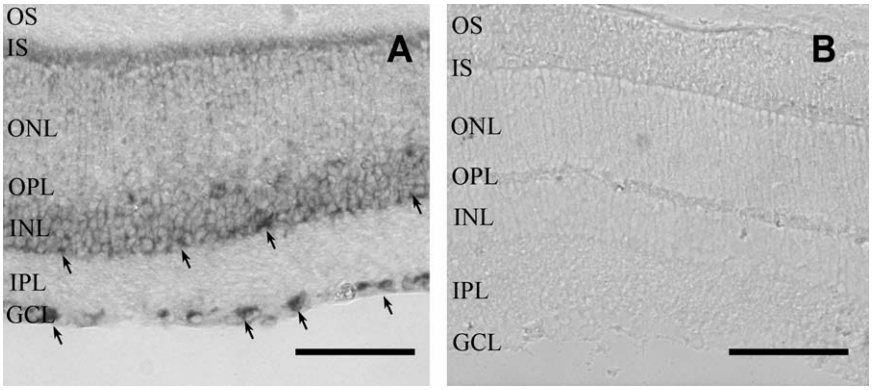

Figure 8. In situ hybridization reveals POMC mRNA in the GCL and INL of wildtype mouse retinas (**A**). Note the dark reaction product obtained with the antisense probe, indicative of POMC mRNA expression in somas located in the GCL and in INL (arrows). **B**: The sense probe failed to label any structure in the retina. OS, photoreceptor outer segment layer; IS, photoreceptor inner segment layer; ONL, outer nuclear layer; OPL, outer plexiform layer; INL, inner nuclear layer; IPL, inner plexiform layer; GCL, ganglion cell layer. Scale bars = 80 μm.

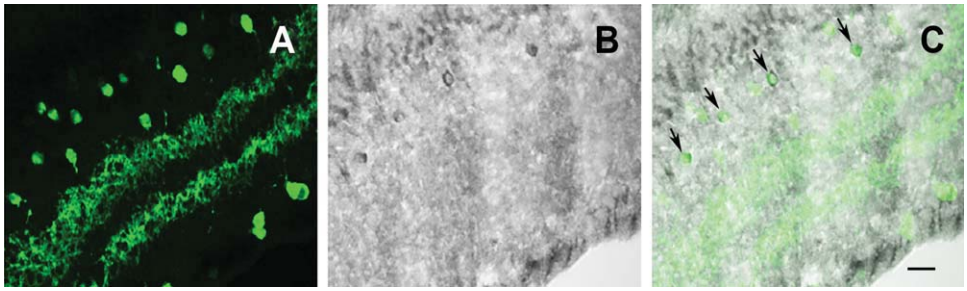

Figure 9. ChAT+ amacrine cells express β-endorphin in the wildtype mouse retina. **A**: A slightly tangential section of wildtype mouse retina showing ChAT+ (green) soma distribution in the INL and GCL together with two bands of immunolabeled processes in the IPL. **B**: DAB amplification of cryostat sectioned retinas for visualization of β-endorphin, illustrating the same region as A. **C**: A merged image of A and B, showing uniform colocalization of β-endorphin+ cell bodies with ChAT+ cells, black arrows. Note that not all ChAT+ cells are β-endorphin+. Scale bar = 20 μm.

mRNA as demonstrated by in situ hybridization. The location of POMC mRNA expressing somas was similar to that of cholinergic amacrine cells, validating the immunohistochemical data. Finally, double-label immunohistochemistry revealed that β-endorphin is present in cholinergic amacrine cells in wildtype mouse retinas. A small fraction of neurons expressing β-endorphin-immunoreactivity was not cholinergic, but we have no further information about these cells beyond their location in inner retina.

Together, the data demonstrate that β-endorphin is expressed in a subset of ChAT+ amacrine cells in the mouse retina. Whether β-endorphin expression marks a functionally distinct subclass of cholinergic amacrine cells across the retina has to be further investigated. The absence of ACTH and α-MSH immunoreactivity in retinal neurons could be secondary to selective processing of POMC at the carboxyl end within these cells. Alternatively, the nonopioid POMC peptides may somehow be selectively degraded or released so they do not achieve detectable levels in the neuronal soma.

Reliability of transgenic mouse lines

Transgenic mouse lines with reporter genes expressed in retinal cells have become an increasingly important tool for extending our knowledge of retinal structure and function. The basic approach is straightforward: couple a fluorophore, such as EGFP, or DsRed in the present case, to a cell-type-specific promoter sequence to achieve reliable, high levels of marker expression in the targeted neuron population. Numerous examples show, however, that the expression pattern of the marker may not match completely the distribution of the targeted cells. Sometimes the transgenic fluorescent signal: 1) cannot be detected in the entire neuron populations as expected based on the natural expression pattern of the promoter (Oliva

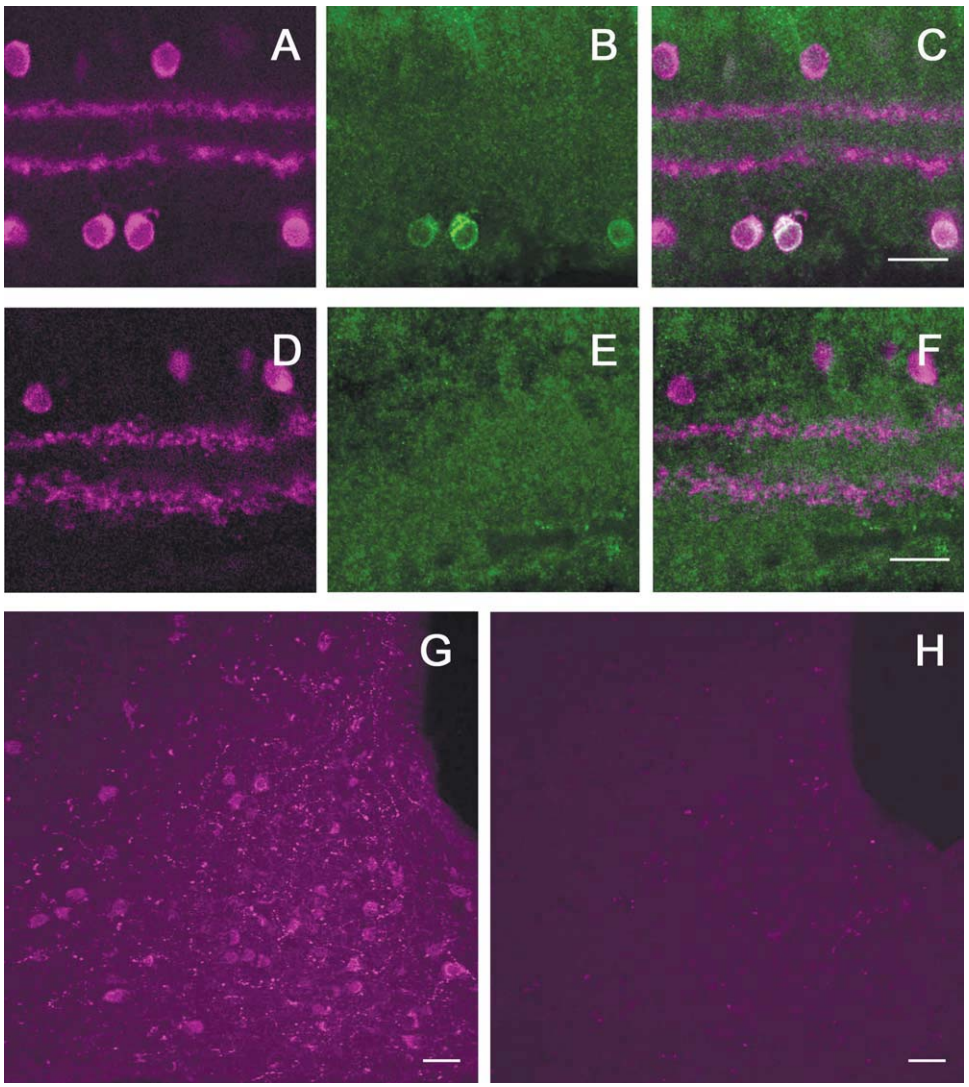

Figure 10. β-Endorphin antibody labeling is specific to POMC neurons in both retina and hypothalamus. **A**: POMC-DsRed (magenta) retina showing DsRed+ soma distribution in both the INL and GCL with two DsRed bands in the IPL. **B**: Same region as in A, showing β-endorphin+ somas within GCL. **C**: A merged image of A and B, showing colocalization of POMC-DsRed+ cell bodies with β-endorphin+ somas. **D**: Vertical cryostat section through POMC-KO retina immunolabeled for ChAT (magenta), showing ChAT+ cell bodies, with two bands in the IPL. **E**: Image illustrating the same area as D, stained with antibodies against β-endorphin (green), showing no specific labeling of somas or projections. **F**: A merged image of D and E, showing only ChAT+ cell bodies and projections. **G**: β-Endorphin immunolabeling (magenta) in the arcuate nucleus of hypothalamus in wildtype mouse. **H**: β-Endorphin immunolabeling (magenta) in the arcuate nucleus of the hypothalamus in POMC KO (*Pomc−/−Tg*) mouse. Scale bars = 20 μm.

et al., 2000); 2) extends beyond the targeted population (Raymond et al., 2008); or 3) localizes to a set of cells completely distinct from the intended targets (Sarthy et al., 2007). These scenarios may even combine when a given transgenic marker expression is compared across different areas of the central nervous system. One example is the ChAT-EGFP mouse line (von Engelhardt at al, 2007) in which transgenic EGFP expression and immunohistochemical ChAT signal showed perfect correspondence in cranial nerve nuclei or in spinal cord motoneurons, but only 35% of ChAT+ striatal, and 42% ChAT+ cortical neurons expressed EGFP. Furthermore, in the retina of this ChAT-EGFP mouse line, although EGFP was expressed by a single amacrine cell population, it was distinct from the population found to be ChAT+ by immunostaining (Haverkamp et al., 2009).

These concerns notwithstanding, retinal transgene expression usually remains constant for a given mouse line. Therefore, studying and characterizing labeled neurons constitute a viable tool that can be used to extend our knowledge of retinal circuitry and function (Raymond et al., 2008; Haverkamp et al., 2009). In the POMC-DsRed

mouse line DsRed signal was consistently expressed in about 50% of ChAT+ amacrines across animals and we found a good correspondence between expression of the transgenic signal (DsRed) and an endogenous product (β-endorphin) in the retina. Thus, the transgenic approach helped us to identify neurons expressing POMC and, in turn, its cleavage product, even though the transgenic POMC-DsRed signal expression exceeded the number of amacrine cells stained for β-endorphin.

The cell counts of DsRed+ neurons underlying the nearest-neighbor analysis established that POMC-expressing amacrine cells are found evenly dispersed in both central and peripheral retina in both orthotopic and displaced layers. However, the regularity of DsRed+ neuron distribution (R) among the population of cholinergic amacrines was higher in the INL than in the GCL (≈3 vs. ≈2, respectively). Spatial pattern analysis performed on the entire population of cholinergic amacrines in the mouse retina (Whitney et al., 2008) revealed a similar difference between the regularity indices calculated from nearest-neighbor distances in the INL and GCL, although at higher overall regularity (4–5 vs. 3, respectively). Based on their detailed analysis Whitney et al. (2008) concluded that even the less regularly packed GCL mosaic of cholinergic cells is nonrandom, representing a degraded version of a more regular, self-spacing mosaic. Based on our nearest-neighbor analysis, POMC-DsRed+ neurons also form a (degraded) regular mosaic as a regularly distributed subpopulation of cholinergic amacrine cells. However, this tentative conclusion needs further testing, since the nearest-neighbor analysis alone is not always enough to discriminate regular spatial mosaics from random distributions (Eglen et al., 2003; Whitney et al., 2008).

The discrepancy in the relative numbers of DsRed+ and β-endorphin+ cells may indicate an asynchronous rhythm in β-endorphin synthesis across the total population of cells. In that regard, in the frog retina β-endorphin expression follows a seasonal rhythm (Jackson et al., 1980). In mammalian retinas, moreover, many genes have been shown to wax and wane on a diurnal or circadian cycle (Storch et al., 2007). Whether β-endorphin production in the mammalian retina is rhythmic remains to be tested.

Opioids may influence retinal function via opioid receptors in the mammalian retina

Opioid binding sites were shown first in rat (Howells et al., 1980), and subsequently in rabbit retina homogenates (Slaughter et al., 1985). In monkey and rat retinas, opioid binding sites are distributed over the IPL and GCL (Wamsley et al., 1981). This is consistent with μ-OR immunoreactivity in the IPL of rat retina, which is associated with bistratified ganglion cells, whose processes ramify in sublaminae 2/3 and 4 (Brecha et al., 1995). A recent report also demonstrated κ- and δ-OR immunofluorescence in the IPL and GCL in rat retina (Husain et al., 2009).

Very little is known about the physiological effects of opioids in the retina. Early studies indicate that enkephalins are released from amacrine cells upon depolarization in a calcium-dependent manner (Su et al., 1983) and inhibit GABA release in the chicken retina (Watt et al., 1984), suggesting that GABAergic amacrine cells possess opioid receptors. Similarly, in goldfish retina exogenous enkephalin enhanced ON ganglion cells spiking plausibly via a disinhibition exerted on GABAergic amacrine cells (Djamgoz et al., 1981). These findings are in accord with the nature of signal transduction pathways linked to the G-protein-coupled μ, κ, or δ opioid receptors (ORs): all three classes have been shown to inhibit adenylate cyclase and voltage-gated calcium channels, or increase inwardly rectifying potassium currents, depending on the studied cell type (see Kieffer, 1995, for review). Although the actual opioid-evoked effects on (GABAergic) amacrine cells are not known, any of the possible opioid actions listed above ultimately leads to inhibition of neuronal activity. Supporting this notion, an ERG study performed in frog and turtle showed that enkephalin agonists produced inhibitory effects (Vitanova et al., 1990).

On the contrary, in isolated rabbit retinas light-evoked acetylcholine release was enhanced by the μ-OR selective agonist [D-Ala^2, MePhe^4, Gly-ol^5]-enkephalin (DAMGO), independent of GABA- or glycine-mediated inhibition (Neal et al., 1994). The same study showed that kainate-induced acetylcholine release is also enhanced by DAMGO. Taken together, a direct, excitatory opioid effect on cholinergic amacrine cells via μ-OR was proposed (Neal et al., 1994). Nevertheless, to explain the DAMGO effect the putative opioid receptors in the rabbit retina should be located presynaptically on cholinergic amacrine cell processes known to arborize around these strata instead of bistratified ganglion cell dendrites as originally reported in the rat (Brecha et al., 1995). Further study is required to determine whether μ-OR agonist DAMGO indeed influences cholinergic amacrine cells directly to enhance acetylcholine release (Neal et al., 1994).

Starburst amacrine cells receive excitatory inputs from bipolar cells, and provide directionally coded inputs to directionally selective ganglion cells (Zhou and Lee, 2008). Whether or not opioids influence the retinal computation for motion detection has not yet been investigated. Opioid receptors have also been implicated in ischemia-induced retinal degeneration. However, at this

point the role of opioid signaling in this regard is somewhat controversial: in one report intraperitoneal application of the nonspecific opioid receptor antagonist, naloxone, prevented ischemic retinal degeneration (Lam et al., 1994), whereas in the other the general opioid receptor agonist, morphine, was found to be beneficial for the survival of ischemia-challenged inner retinal neurons (Husain et al., 2009). Hypoxic preconditioning also led to upregulation of δ-OR in rat retinas (Peng et al., 2009).

In summary, we have shown that a large fraction of cholinergic amacrine cells, which have a fundamental role in processing information about motion within the mammalian retina (Zhou and Lee, 2008), express β-endorphin. The relevant receptor for β-endorphin, the μ-OR, is reported to be located on ganglion cell dendrites within the IPL (Brecha et al., 1995), which places them in close spatial apposition to the sites of β-endorphin release. Although functional data are lacking, these anatomical findings suggest a role for β-endorphin in ganglion cell signal processing, analogous to what has been reported for other retinal peptides (Zalutsky and Miller, 1990a,b).

ACKNOWLEDGMENT

The authors thank Kizzy English for technical assistance and Carol Mura and Muriel Philipps from Eurexpress for their help in setting up the in situ hybridization.

LITERATURE CITED

Altschuler RA, Mosinger JL, Hoffman DW, Parakkal MH. 1982. Immunocytochemical localization of enkephalin-like immunoreactivity in the retina of the guinea pig. Proc Natl Acad Sci USA 79:2398–2400.

Andrade da Costa BL, Hokoc JN. 2003. Coexistence of GAD-65 and GAD-67 with tyrosine hydroxylase and nitric oxide synthase in amacrine and interplexiform cells of the primate, Cebus apella. Vis Neurosci 20:153–163.

Bicknell AB. 2008. The tissue-specific processing of pro-opiomelanocortin. J Neuroendocrinol 20:692–699.

Borbe HO, Wollert U, Muller WE. 1982. Stereospecific [3H]naloxone binding associated with opiate receptors in bovine retina. Exp Eye Res 34:539–544.

Brecha NC. 2003. Peptide and peptide receptor expression and function in the vertebrate retina. In: Chalupa, Werner, editors. The visual neurosciences. Cambridge, MA: MIT Press. p 334–354.

Brecha NC, Johnson J, Kui B, Anton B, Keith D, Evans C, Sternini C. 1995. Mu opioid receptor immunoreactivity is expressed in the retina and retina recipient nuclei. Analgesia 1:331–334.

Brunelli G, Spano P, Barlati S, Guarneri B, Barbon A, Bresciani R, Pizzi M. 2005. Glutamatergic reinnervation through peripheral nerve graft dictates assembly of glutamatergic synapses at rat skeletal muscle. Proc Natl Acad Sci USA 102:8752–8757.

Campbell RE, Tour O, Palmer AE, Steinbach PA, Baird GS, Zacharias DA, Tsien RY. 2002. A monomeric red fluorescent protein. Proc Natl Acad Sci USA 99:7877–7882.

Caputi A, Rozov A, Blatow M, Monyer H. 2009. Two calretinin-positive GABAergic cell types in layer 2/3 of the mouse neocortex provide different forms of inhibition. Cereb Cortex 19:1345–1359.

Casini G, Brecha NC. 1992. Colocalization of vasoactive intestinal polypeptide and GABA immunoreactivities in a population of wide-field amacrine cells in the rabbit retina. Vis Neurosci 8:373–378.

Chang YC, Gottlieb DI. 1988. Characterization of the proteins purified with monoclonal antibodies to glutamic acid decarboxylase. J Neurosci 8:2123–2130.

Chen P, Williams SM, Grove KL, Smith MS. 2004. Melanocortin 4 receptor-mediated hyperphagia and activation of neuropeptide Y expression in the dorsomedial hypothalamus during lactation. J Neurosci 24:5091–6100.

Choi JH, Lee CH, Yoo KY, Hwang IK, Lee IS, Lee YL, Shin HC, Won MH. 2010. Age-related changes in calbindin-D28k, parvalbumin, and calretinin immunoreactivity in the dog main olfactory bulb. Cell Mol Neurobiol 30:1–12.

Cuenca N, Kolb H. 1998. Circuitry and role of substance P-immunoreactive neurons in the primate retina. J Comp Neurol 393:439–456.

de Melo J, Du G, Fonseca M, Gillespie LA, Turk WJ, Rubenstein JL, Eisenstat DD. 2005. Dlx1 and Dlx2 function is necessary for terminal differentiation and survival of late-born retinal ganglion cells in the developing mouse retina. Development 132:311–322.

de Souza FS, Santangelo AM, Bumaschny V, Avale ME, Smart JL, Low MJ, Rubinstein M. 2005. Identification of neuronal enhancers of the proopiomelanocortin gene by transgenic mouse analysis and phylogenetic footprinting. Mol Cell Biol 25:3076–3086.

Djamgoz MB, Stell WK, Chin CA, Lam DM. 1981. An opiate system in the goldfish retina. Nature 292:620–623.

Dkhissi O, Julien JF, Wasowicz M, il-Thiney N, Nguyen-Legros J, Versaux-Botteri C. 2001. Differential expression of GAD(65) and GAD(67) during the development of the rat retina. Brain Res 919:242–249.

Eglen SJ, Raven MA, Tamrazian E, Reese BE. 2003. Dopaminergic amacrine cells in the inner nuclear layer and ganglion cell layer comprise a single functional retinal mosaic. J Comp Neurol 466:343–355.

Ehinger B. 1982. Neurotransmitter systems in the retina. Retina 2:305–221.

Elias CF, Saper CB, Maratos-Flier E, Tritos NA, Lee C, Kelly J, Tatro JB, Hoffman GE, Ollmann MM, Barsh GS, Sakurai T, Yanagisawa M, Elmquist JK. 1998. Chemically defined projections linking the mediobasal hypothalamus and the lateral hypothalamic area. J Comp Neurol 402:442–459.

Fischer AJ, Seltner RL, Stell WK. 1998. Opiate and N-methyl-D-aspartate receptors in form-deprivation myopia. Vis Neurosci 15:1089–10896.

Gábriel R, Volgyi B, Pollak E. 1998. Calretinin-immunoreactive elements in the retina and optic tectum of the frog, Rana esculenta. Brain Res 782:53–62.

Ghosh KK, Bujan S, Haverkamp S, Feigenspan A, Wässle H. 2004. Types of bipolar cells in the mouse retina. J Comp Neurol 469:70–82.

Hamano K, Kiyama H, Emson PC, Manabe R, Nakauchi M, Tohyama M. 1990. Localization of two calcium binding proteins, calbindin (28 kD) and parvalbumin (12 kD), in the vertebrate retina. J Comp Neurol 302:417–424.

Hannibal J, Moller M, Ottersen OP, Fahrenkrug J. 2000. PACAP and glutamate are co-stored in the retinohypothalamic tract. J Comp Neurol 418:147–155.

Haverkamp S, Wässle H. 2000. Immunocytochemical analysis of the mouse retina. J Comp Neurol 424:1–23.

Haverkamp S, Inta D, Monyer H, Wässle H. 2009. Expression analysis of green fluorescent protein in retinal neurons of four transgenic mouse lines. Neuroscience 160:126–139.

Hentges ST, Otero-Corchon V, Pennock RL, King CM, Low MJ. 2009. Proopiomelanocortin expression in both GABA and glutamate neurons. J Neurosci 29:13684–13690.

Hokfelt T, Broberger C, Xu ZQ, Sergeyev V, Ubink R, Diez M. 2000. Neuropeptides—an overview. Neuropharmacology 39:1337–1356.

Howells RD, Groth J, Hiller JM, Simon EJ. 1980. Opiate binding sites in the retina: properties and distribution. J Pharmacol Exp Ther 215:60–64.

Husain S, Potter DE, Crosson CE. 2009. Opioid receptor-activation: retina protected from ischemic injury. Invest Ophthalmol Vis Sci 50:3853–3859.

Jackson IM, Bolaffi JL, Guillemin R. 1980. Presence of immunoreactive beta-endorphin and enkephalin-like material in the retina and other tissues of the frog, Rana pipiens. Gen Comp Endocrinol 42:505–508.

Jeon CJ, Strettoi E, Masland RH. 1998. The major cell populations of the mouse retina. J Neurosci 18:8936–8946.

Kang TH, Ryu YH, Kim IB, Oh GT, Chun MH. 2004. Comparative study of cholinergic cells in retinas of various mouse strains. Cell Tissue Res 317:109–115.

Khalap A, Bagrosky B, Lecaude S, Youson J, Danielson P, Dores RM. 2005. Trends in the evolution of the proenkephalin and prodynorphin genes in gnathostomes. Ann NY Acad Sci 1040:22–37.

Kieffer BL. 1995. Recent advances in molecular recognition and signal transduction of active peptides: receptors for opioid peptides. Cell Mol Neurobiol 15:615–635.

Kielczewski JL, Pease ME, Quigley HA. 2005. The effect of experimental glaucoma and optic nerve transection on amacrine cells in the rat retina. Invest Ophthalmol Vis Sci 46: 3188–3196.

Kong JH, Fish DR, Rockhill RL, Masland RH. 2005. Diversity of ganglion cells in the mouse retina: unsupervised morphological classification and its limits. J Comp Neurol 489:293–310.

Lam TT, Takahashi K, Tso MO. 1994. The effects of naloxone on retinal ischemia in rats. J Ocul Pharmacol 10:481–492.

MacNeil MA, Masland RH. 1998. Extreme diversity among amacrine cells: implications for function. Neuron 20: 971–982.

Marc RE, Murry RF, Fisher SK, Linberg KA, Lewis GP, Kalloniatis M. 1998. Amino acid signatures in the normal cat retina. Invest Ophthalmol Vis Sci 39:1685–1693.

Masland RH, Mills JW. 1979. Autoradiographic identification of acetylcholine in the rabbit retina. J Cell Biol 83:159–178.

Matilla A, Gorbea C, Einum DD, Townsend J, Michalik A, van BC, Jensen CC, Murphy KJ, Ptacek LJ, Fu YH. 2001. Association of ataxin-7 with the proteasome subunit S4 of the 19S regulatory complex. Hum Mol Genet 10:2821–2831.

May CA, Nakamura K, Fujiyama F, Yanagawa Y. 2008. Quantification and characterization of GABA-ergic amacrine cells in the retina of GAD67-GFP knock-in mice. Acta Ophthalmol 86:395–400.

Medzihradsky F. 1976. Stereospecific binding of etorphine in isolated neural cells and in retina, determined by a sensitive microassay. Brain Res 108:212–219.

Millington GW. 2007. The role of proopiomelanocortin (POMC) neurones in feeding behaviour. Nutr Metab (Lond) 4:18.

Moon JI, Kim IB, Gwon JS, Park MH, Kang TH, Lim EJ, Choi KR, Chun MH. 2005. Changes in retinal neuronal populations in the DBA/2J mouse. Cell Tissue Res 320:51–59.

Neal MJ, Paterson SJ, Cunningham JR. 1994. Enhancement of retinal acetylcholine release by DAMGO: possibly a direct opioid receptor-mediated excitatory effect. Br J Pharmacol 113:789–794.

Oliva AA Jr, Jiang M, Lam T, Smith KL, Swann JW. 2000. Novel hippocampal interneuronal subtypes identified using transgenic mice that express green fluorescent protein in GABAergic interneurons. J Neurosci 20:3354–3368.

Overstreet LS, Hentges ST, Bumaschny VF, de Souza FS, Smart JL, Santangelo AM, Low MJ, Westbrook GL, Rubinstein M. 2004. A transgenic marker for newly born granule cells in dentate gyrus. J Neurosci 24:3251–3259.

Peng PH, Huang HS, Lee YJ, Chen YS, Ma MC. 2009. Novel role for the delta-opioid receptor in hypoxic preconditioning in rat retinas. J Neurochem 108:741–754.

Pow DV. 1998. Transport is the primary determinant of glycine content in retinal neurons. J Neurochem 70:2628–2636.

Raymond ID, Vila A, Huynh UC, Brecha NC. 2008. Cyan fluorescent protein expression in ganglion and amacrine cells in a thy1-CFP transgenic mouse retina. Mol Vis 14:1559–1574.

Sarthy V, Hoshi H, Mills S, Dudley VJ. 2007. Characterization of green fluorescent protein-expressing retinal cells in CD 44-transgenic mice. Neuroscience 144:1087–1093.

Seltner RL, Rohrer B, Grant V, Stell WK. 1997. Endogenous opiates in the chick retina and their role in form-deprivation myopia. Vis Neurosci 14:801–809.

Slaughter MM, Mattler JA, Gottlieb DI. 1985. Opiate binding sites in the chick, rabbit and goldfish retina. Brain Res 339:39–47.

Smart JL, Tolle V, Low MJ. 2006. Glucocorticoids exacerbate obesity and insulin resistance in neuron-specific proopiomelanocortin-deficient mice. J Clin Invest 116:495–505.

Storch KF, Paz C, Signorovitch J, Raviola E, Pawlyk B, Li T, Weitz CJ. 2007. Intrinsic circadian clock of the mammalian retina: importance for retinal processing of visual information. Cell 130:730–741.

Su YY, Watt CB, Lam DM. 1985. Opioid pathways in an avian retina. I. The content, biosynthesis, and release of Met5-enkephalin. J Neurosci 5:851–856.

Tamamaki N, Yanagawa Y, Tomioka R, Miyazaki J, Obata K, Kaneko T. 2003. Green fluorescent protein expression and colocalization with calretinin, parvalbumin, and somatostatin in the GAD67-GFP knock-in mouse. J Comp Neurol 467:60–79.

Vaney DI, Whitington GE, Young HM. 1989. The morphology and topographic distribution of substance-P-like immunoreactive amacrine cells in the cat retina. Proc R Soc Lond B Biol Sci 237:471–488.

Vaney DI, Nelson JC, Pow DV. 1998. Neurotransmitter coupling through gap junctions in the retina. J Neurosci 18: 10594–10602.

Vardi N, Auerbach P. 1995. Specific cell types in cat retina express different forms of glutamic acid decarboxylase. J Comp Neurol 351:374–384.

Vitanova L, Popova E, Kupenova P, Kosteljanetz N, Belcheva S. 1990. Comparative studies on the effects of some enkephalin agonists on the ERG of frog and turtle. Comp Biochem Physiol C 97:93–98.

Voigt T. 1986. Cholinergic amacrine cells in the rat retina. J Comp Neurol 248:19–35.

von Engelhardt J, Eliava M, Meyer AH, Rozov A, Monyer H. 2007. Functional characterization of intrinsic cholinergic interneurons in the cortex. J Neurosci 27:5633–5642.

Wamsley JK, Palacios JM, Kuhar MJ. 1981. Autoradiographic localization of opioid receptors in the mammalian retina. Neurosci Lett 27:19–24.

Wässle H, Riemann HJ. 1978. The mosaic of nerve cells in the mammalian retina. Proc R Soc Lond B Biol Sci 200: 441–461.

Watt CB, Su YY, Lam DM. 1984. Interactions between enkephalin and GABA in avian retina. Nature 311: 761–763.

Watt CB, Li T, Lam DM, Wu SM. 1988. Quantitative studies of enkephalin's coexistence with gamma-aminobutyric acid, glycine and neurotensin in amacrine cells of the chicken retina. Brain Res 444:366–370.

Whitney IE, Keeley PW, Raven MA, Reese BE. 2008. Spatial patterning of cholinergic amacrine cells in the mouse retina. J Comp Neurol 508:1–12.

Yamamoto T, Yamato E, Tashiro F, Sato T, Noso S, Ikegami H, Tamura S, Yanagawa Y, Miyazaki JI. 2004. Development of autoimmune diabetes in glutamic acid decarboxylase 65 (GAD65) knockout NOD mice. Diabetologia 47:221–224.

Yamasaki EN, Barbosa VD, De Mello FG, Hokoc JN. 1999. GABAergic system in the developing mammalian retina: dual sources of GABA at early stages of postnatal development. Int J Dev Neurosci 17:201–213.

Yang DS, Boelen MK, Morgan IG. 1997. Development of the enkephalin-, neurotensin- and somatostatin-like (ENSLI) amacrine cells in the chicken retina. Brain Res Dev Brain Res 101:57–65.

Zafra F, Aragon C, Olivares L, Danbolt NC, Gimenez C, Storm-Mathisen J. 1995. Glycine transporters are differentially expressed among CNS cells. J Neurosci 15(5 Pt 2): 3952–3969.

Zalutsky RA, Miller RF. 1990a. The physiology of somatostatin in the rabbit retina. J Neurosci 10:383–393.

Zalutsky RA, Miller RF. 1990b. The physiology of substance P in the rabbit retina. J Neurosci 10:394–402.

Zhou ZJ, Lee S. 2008. Synaptic physiology of direction selectivity in the retina. J Physiol 586(Pt 18): 4371–4376.